

# A time-series approach to dynamical systems from classical and quantum worlds

Ruben Fossion

Citation: [AIP Conference Proceedings](#) **1575**, 89 (2014); doi: 10.1063/1.4861700

View online: <http://dx.doi.org/10.1063/1.4861700>

View Table of Contents: <http://aip.scitation.org/toc/apc/1575/1>

Published by the [American Institute of Physics](#)

---

## Articles you may be interested in

[Diagnosis of digestive functional disease by the statistics of continuous monitoring of esophageal acidity](#)

[AIP Conference Proceedings](#) **1626**, 185 (2015); 10.1063/1.4901389

---

# A time-series approach to dynamical systems from classical and quantum worlds

Ruben Fossion

*Instituto Nacional de Geriatria, Periférico Sur No. 2767, Col. San Jerónimo Lídice,  
Del. Magdalena Contreras, 10200 México D.F., Mexico  
Centro de Ciencias de la Complejidad (C3), Universidad Nacional Autónoma de México,  
04510 México, D.F., Mexico*

**Abstract.** This contribution discusses some recent applications of time-series analysis in Random Matrix Theory (RMT), and applications of RMT in the statistical analysis of eigenspectra of correlation matrices of multivariate time series.

## 1. INTRODUCTION

Time-series analysis and Random Matrix Theory (RMT) used to be two different fields. In recent years, however, there have been interesting applications of time-series analysis in RMT, and vice versa. Time-series analysis is an approach to complex systems where the dynamics of the system is inferred by a statistical analysis of the fluctuations in time of some associated observable. Random Matrix Theory (RMT) is a standard technique in the study of quantum chaos, which includes the statistical study of the excitation spectrum of a dynamical quantum system. In this contribution, some examples of these mutual applications are given.

This contribution consists of four sections. In the first section, a standard technique to study multivariate time series is described, namely Singular Value Decomposition (SVD), which can be considered as a generalization of standard matrix spectral decomposition generalized for non-symmetric rectangular matrices. In the second section, Random Matrix Theory (RMT) and its relevance to the statistical study of quantum excitation spectra is briefly discussed. In the third section, two recent applications of time-series analysis to RMT are mentioned: a first application applies time-series analysis as a fluctuation measure for quantum excitation states, and a second application permits to separate in a data-adaptive way the global trend of a quantum excitation spectrum from the local fluctuations. In the fourth section, RMT is used to extract statistical information from the eigen-spectrum of the correlation matrix of a multivariate time series.

## 2. MULTIVARIATE TIME SERIES

### 2.1. Spectral decomposition of square matrices

#### 2.1.1. Right (column) eigenvectors

Let  $\mathbf{A}$  be a real symmetric matrix with dimensions  $N \times N$ . Let the rank of the matrix be  $r = \text{rank}(\mathbf{A}) \leq N$ , which is equal to the number of independent columns, and also equal to the number of independent rows. If we represent vectors as columns, then these should be placed to the right side of  $\mathbf{A}$ . For each  $\vec{v}_k$  right (column) eigenvector of  $\mathbf{A}$ , with  $k = 1 \dots r$ , we have then,

$$\mathbf{A}\vec{v}_k = \lambda \vec{v}_k, \quad (1)$$

or explicitly, for  $N = 2$ ,

$$\begin{pmatrix} A_{11} & A_{12} \\ A_{21} & A_{22} \end{pmatrix} \begin{pmatrix} v_{k1} \\ v_{k2} \end{pmatrix} = \lambda \begin{pmatrix} v_{k1} \\ v_{k2} \end{pmatrix} \quad (2)$$

The right (column) eigenvectors  $\vec{v}_k$  constitute an orthonormal basis for the column space  $\mathbb{R}^r$  of  $\mathbf{A}$ , i.e.  $\vec{v}_k \cdot \vec{v}_l = \delta_{kl}$ , with  $k, l = 1 \dots r$ . We can represent the eigenvectors as the columns of the  $N \times N$  dimensional matrix  $\mathbf{V}$ , and the associated eigenvalues  $\lambda_k$  as the elements of the  $N \times N$  dimensional diagonal matrix  $\mathbf{\Sigma}$  (the last  $N - r$  rows and columns can be padded with zeros), so that the relation between matrix  $\mathbf{A}$  and its eigenvectors can be noted in a compact matrix form as,

$$\mathbf{A}\mathbf{V} = \mathbf{V}\mathbf{\Lambda}, \quad (3)$$

or, explicitly, for  $N = r = 2$ , and eigenvectors  $\vec{v}_1 = (v_{11}, v_{12})^T$  and  $\vec{v}_2 = (v_{21}, v_{22})^T$ ,

$$\begin{aligned} \begin{pmatrix} A_{11} & A_{12} \\ A_{21} & A_{22} \end{pmatrix} \begin{pmatrix} \begin{pmatrix} v_{11} \\ v_{12} \end{pmatrix} & \begin{pmatrix} v_{21} \\ v_{22} \end{pmatrix} \end{pmatrix} &= \begin{pmatrix} \begin{pmatrix} v_{11} \\ v_{12} \end{pmatrix} & \begin{pmatrix} v_{21} \\ v_{22} \end{pmatrix} \end{pmatrix} \begin{pmatrix} \lambda_1 & 0 \\ 0 & \lambda_2 \end{pmatrix} \\ &= \begin{pmatrix} \begin{pmatrix} \lambda_1 v_{11} \\ \lambda_1 v_{12} \end{pmatrix} & \begin{pmatrix} \lambda_2 v_{21} \\ \lambda_2 v_{22} \end{pmatrix} \end{pmatrix}. \end{aligned} \quad (4)$$

Starting from eq. (3), matrix  $\mathbf{A}$  can be rewritten as a spectral decomposition,

$$\begin{aligned} \mathbf{A} &= \mathbf{V}\mathbf{\Lambda}\mathbf{V}^T \\ &= \sum_{k=1}^r \lambda_k (\vec{v}_k \vec{v}_k^T) = \sum_{k=1}^r \lambda_k A_k, \end{aligned} \quad (5)$$

where we made use of the fact that  $\mathbf{V}$  is an orthogonal matrix so that  $\mathbf{V}^{-1} = \mathbf{V}^T$ , and where  $A_k = \vec{v}_k \vec{v}_k^T = \vec{v}_k \otimes \vec{v}_k$  is the vector outside (tensor) product. The  $r$ -dimensional column space of  $\mathbf{A}$  is decomposed as the direct sum of the 1-dimensional orthogonal vector spaces spanned by the  $r$  eigenvectors  $\vec{v}_k$ ,  $\mathbb{R}^r = \mathbb{R}_1 \oplus \mathbb{R}_2 \oplus \dots \mathbb{R}_r$ . Explicitly, for

the case  $N = r = 2$ , we have

$$\begin{aligned}
\begin{pmatrix} A_{11} & A_{12} \\ A_{21} & A_{22} \end{pmatrix} &= \left( \begin{pmatrix} v_{11} \\ v_{12} \end{pmatrix} \begin{pmatrix} v_{21} \\ v_{22} \end{pmatrix} \right) \begin{pmatrix} \lambda_1 & 0 \\ 0 & \lambda_2 \end{pmatrix} \begin{pmatrix} (v_{11} & v_{12}) \\ (v_{21} & v_{22}) \end{pmatrix} \\
&= \begin{pmatrix} \lambda_1 v_{11}^2 + \lambda_2 v_{21}^2 & \lambda_1 v_{11} v_{12} + \lambda_2 v_{21} v_{22} \\ \lambda_1 v_{11} v_{12} + \lambda_2 v_{21} v_{22} & \lambda_1 v_{12}^2 + \lambda_2 v_{22}^2 \end{pmatrix} \\
&= \lambda_1 \begin{pmatrix} v_{11}^2 & v_{11} v_{12} \\ v_{11} v_{12} & v_{12}^2 \end{pmatrix} + \lambda_2 \begin{pmatrix} v_{21}^2 & v_{21} v_{22} \\ v_{21} v_{22} & v_{22}^2 \end{pmatrix} \\
&= \lambda_1 A_1 + \lambda_2 A_2,
\end{aligned} \tag{6}$$

taking into account that the vector outer (tensorial) product  $\vec{v}_k \vec{v}_k^T$  can be written as,

$$\begin{pmatrix} v_{k1} \\ v_{k2} \end{pmatrix} \begin{pmatrix} v_{k1} & v_{k2} \end{pmatrix} = \begin{pmatrix} v_{k1}^2 & v_{k1} v_{k2} \\ v_{k1} v_{k2} & v_{k2}^2 \end{pmatrix}. \tag{7}$$

### 2.1.2. Left (row) eigenvectors

Similar to the previous section, we now study the left (row) eigenvectors  $\vec{u}_k$  of the real symmetric matrix  $\mathbf{A}$  with dimension  $N \times N$  and rank  $r$ . Thus, we have,

$$\vec{u}_k \mathbf{A} = \lambda \vec{u}_k, \tag{8}$$

or explicitly, for  $N = 2$ ,

$$\begin{pmatrix} u_{k1} & u_{k2} \end{pmatrix} \begin{pmatrix} A_{11} & A_{12} \\ A_{21} & A_{22} \end{pmatrix} = \lambda \begin{pmatrix} u_{k1} & u_{k2} \end{pmatrix}. \tag{9}$$

The left (row) eigenvectors  $\vec{u}_k$  constitute an orthonormal basis for the row space  $\mathbb{R}^r$  of  $\mathbf{A}$ , i.e.  $\vec{u}_k \cdot \vec{u}_l = \delta_{kl}$ , with  $k, l = 1 \dots r$ . The eigenvectors  $\vec{u}_k$  can be represented as the rows of a  $N \times N$  dimensional matrix  $\mathbf{U}$ , and the associated eigenvalues  $\lambda_k$  as the elements of a  $N \times N$  dimensional diagonal matrix  $\mathbf{\Sigma}$  (the last  $N - r$  rows and columns can be padded with zeros), so that the relation between matrix  $\mathbf{A}$  and its eigenvectors can be noted in a compact matrix form as,

$$\mathbf{U} \mathbf{A} = \mathbf{\Lambda} \mathbf{U}, \tag{10}$$

or, explicitly, for  $N = r = 2$ , and eigenvectors  $\vec{u}_1 = (u_{11}, u_{12})$  and  $\vec{u}_2 = (u_{21}, u_{22})^T$ ,

$$\begin{aligned}
\begin{pmatrix} (u_{11} & u_{12}) \\ (u_{21} & u_{22}) \end{pmatrix} \begin{pmatrix} A_{11} & A_{12} \\ A_{21} & A_{22} \end{pmatrix} &= \begin{pmatrix} \lambda_1 & 0 \\ 0 & \lambda_2 \end{pmatrix} \begin{pmatrix} (u_{11} & u_{12}) \\ (u_{21} & u_{22}) \end{pmatrix} \\
&= \begin{pmatrix} (\lambda_1 u_{11} & \lambda_1 u_{12}) \\ (\lambda_2 u_{21} & \lambda_2 u_{22}) \end{pmatrix}.
\end{aligned} \tag{11}$$

Starting from eq. (10), matrix  $\mathbf{A}$  can be rewritten as a spectral decomposition,

$$\begin{aligned}\mathbf{A} &= \mathbf{U}^T \mathbf{\Lambda} \mathbf{U} \\ &= \sum_{k=1}^r \lambda_k (\vec{u}_k^T \vec{u}_k) = \sum_{k=1}^r \lambda_k A_k,\end{aligned}\quad (12)$$

where we made use of the fact that  $\mathbf{U}$  is an orthogonal matrix so that  $\mathbf{U}^{-1} = \mathbf{U}^T$ , and where  $A_k = \vec{u}_k^T \vec{u}_k = \vec{u}_k \otimes \vec{u}_k$  is the vector outside (tensor) product. The  $r$ -dimensional row space of  $\mathbf{A}$  is decomposed as the direct sum of the 1-dimensional orthogonal vector spaces spanned by the  $r$  eigenvectors  $\vec{u}_k$ ,  $\mathbb{R}^r = \mathbb{R}_1 \oplus \mathbb{R}_2 \oplus \dots \mathbb{R}_r$ . Explicitly, for the case  $N = r = 2$ , we have

$$\begin{aligned}\begin{pmatrix} A_{11} & A_{12} \\ A_{21} & A_{22} \end{pmatrix} &= \begin{pmatrix} \begin{pmatrix} u_{11} \\ u_{21} \end{pmatrix} \begin{pmatrix} u_{12} \\ u_{22} \end{pmatrix} \end{pmatrix} \begin{pmatrix} \lambda_1 & 0 \\ 0 & \lambda_2 \end{pmatrix} \begin{pmatrix} \begin{pmatrix} u_{11} & u_{21} \end{pmatrix} \\ \begin{pmatrix} u_{12} & u_{22} \end{pmatrix} \end{pmatrix} \\ &= \begin{pmatrix} \lambda_1 u_{11}^2 + \lambda_2 u_{12}^2 & \lambda_1 u_{11} u_{21} + \lambda_2 u_{12} u_{22} \\ \lambda_1 u_{11} u_{21} + \lambda_2 u_{12} u_{22} & \lambda_1 u_{21}^2 + \lambda_2 u_{22}^2 \end{pmatrix} \\ &= \lambda_1 \begin{pmatrix} u_{11}^2 & u_{11} u_{21} \\ u_{11} u_{21} & u_{21}^2 \end{pmatrix} + \lambda_2 \begin{pmatrix} u_{12}^2 & u_{12} u_{22} \\ u_{12} u_{22} & u_{22}^2 \end{pmatrix} \\ &= \lambda_1 A_1 + \lambda_2 A_2,\end{aligned}\quad (13)$$

taking into account that the vector outer (tensorial) product  $\vec{u}_k^T \vec{u}_k$  can be written as,

$$\begin{pmatrix} u_{k1} \\ u_{k2} \end{pmatrix} \begin{pmatrix} u_{k1} & u_{k2} \end{pmatrix} = \begin{pmatrix} u_{k1}^2 & u_{k1} u_{k2} \\ u_{k1} u_{k2} & u_{k2}^2 \end{pmatrix}.\quad (14)$$

## 2.2. Generalized spectral decomposition for rectangular matrices

### 2.2.1. Singular Value Decomposition (SVD)

Consider a real rectangular and orthogonal matrix  $\mathbf{X}$  of dimension  $M \times N$  of rank  $r = \text{rank}(\mathbf{X}) \leq \text{Min}(M, N)$ . The matrix can be used to store in its rows a multivariate time series corresponding to the time evolution  $f^{(m)}(n)$  of  $m = 1 \dots M$  observables over a time length  $n = 1 \dots N$ . Often, the individual time series are normalized as  $(f^{(m)} - \langle f^{(m)} \rangle) / \sigma^{(m)}$ , where  $\langle f^{(m)} \rangle$  and  $\sigma^{(m)}$  are the mean and the standard deviation of each individual time series. The spectral decomposition of square matrices of eq. (5) and (12) can be generalized to the Singular Value Decomposition (SVD) valid for rectangular matrices, see Fig. 1,

$$\mathbf{X} = \mathbf{U} \mathbf{\Sigma} \mathbf{V}^T = \sum_{k=1}^r \sigma_k \vec{u}_k \vec{v}_k^T = \sum_{k=1}^r \sigma_k \mathbf{X}_k,\quad (15)$$

where the  $M \times M$  matrix  $\mathbf{U}$  contains in its columns the left singular vectors  $\vec{u}_k$ , the  $N \times N$  matrix  $\mathbf{V}$  contains in its columns the right singular vectors  $\vec{v}_k$ , the  $M \times N$  matrix  $\mathbf{\Sigma}$

is diagonal and contains the ordered singular values  $\sigma_1 \geq \sigma_2 \geq \dots \geq \sigma_r$ . Here also,  $\mathbf{X}_k = \vec{u}_k \vec{v}_k^T \equiv \vec{u}_k \otimes \vec{v}_k$  are elementary (rank-1) matrices.

The orthonormal set  $\vec{v}_k \vec{v}_l^T = \delta_{kl}$  constitutes a basis for the row space of  $\mathbf{X}$ . In the present application, the row space of  $\mathbf{X}$  has a physical interpretation as it represents the time evolution of the multivariate time series. Note that the eigenvectors  $\vec{v}_k = (v_{1k}, v_{2k} \dots v_{Nk})$  have the same length  $N$  as each of the individual time series  $f^{(m)}(n)$  with  $n = 1 \dots N$ . Thus, the eigenvectors  $\vec{v}_k$  can be interpreted as temporal eigen-modes of  $\mathbf{X}$ .

On the other hand, the orthonormal set  $\vec{u}_k \vec{u}_l^T = \delta_{kl}$  constitutes a basis for the column space of  $\mathbf{X}$ . The column space now also has a physical interpretation. A column of  $\mathbf{X}$  consists of the measurements  $f^{(m)}(n_0)$  of the  $m = 1 \dots M$  observables at time moment  $n = n_0$ , and thus constitutes a static snapshot of how the different observables relate at that specific time moment. Each column can be interpreted as the spatial configuration of the  $m = 1 \dots M$  observables at each time moment. Thus the vectors  $\vec{u}_k = (u_{k1}, u_{k2} \dots u_{kM})$  constitute the spatial eigen-modes of  $\mathbf{X}$ .

In the case of symmetrical matrices,  $\mathbf{X} = \mathbf{X}^T$ , it can be seen that  $\mathbf{U}\mathbf{\Sigma}\mathbf{V}^T = \mathbf{V}\mathbf{\Sigma}^T\mathbf{U}^T$ , so that left and right singular vectors are the same,  $\vec{u}_k = \vec{v}_k$ , and SVD can be considered as an eigen-decomposition generalized to rectangular matrices. Many mathematical software packages, such as e.g. Mathematica, contain routines that readily print out the SVD decomposition of a matrix. However, the actual calculation of the singular vectors  $\vec{u}_k, \vec{v}_k$  and singular values  $\sigma_k$  is done using two associated correlation matrices.

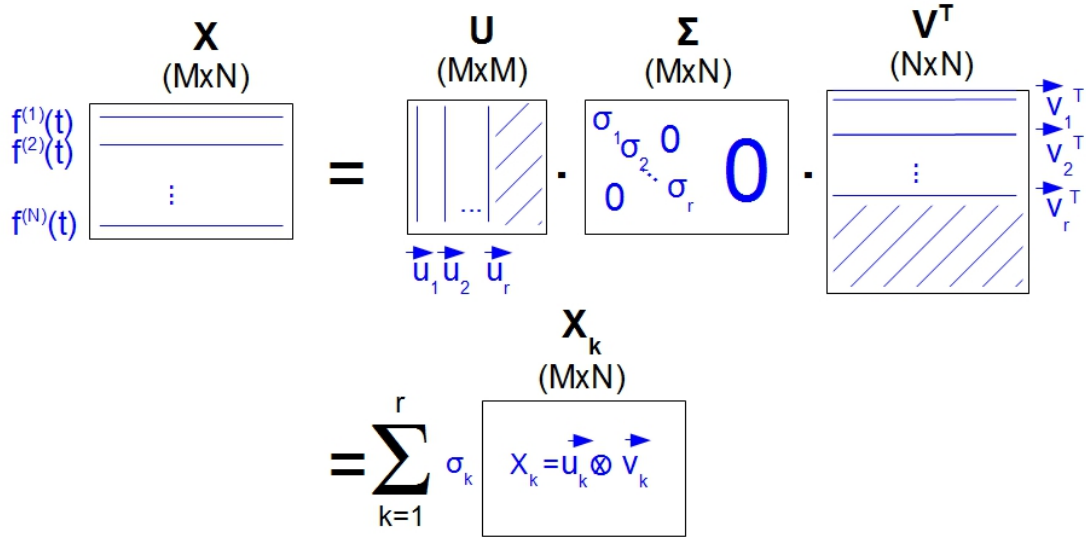


**FIGURE 1.** Singular Value Decomposition (SVD) of a rectangular data matrix  $\mathbf{X}$  with dimensions  $M \times N$  and  $r = \text{rank}(\mathbf{X}) \leq \text{Min}(M, N)$ , see eq. (15). Each row of  $\mathbf{X}$  contains one of  $m = 1 \dots M$  time series  $f^{(m)}(n)$  with length  $n = 1 \dots N$ . The left (right) singular vectors  $\vec{u}_k$  ( $\vec{v}_k$ ) constitute the spatial (temporal) eigen-modes of the multivariate time series  $\mathbf{X}$ , and the ordered singular values  $\sigma_1 \geq \sigma_2 \geq \dots \geq \sigma_R$  are the associated weights.

### 2.2.2. Spatial correlation matrix

The spatial correlation matrix is defined as

$$\mathbf{S}_s = \frac{1}{N} \mathbf{X} \mathbf{X}^T, \quad (16)$$

with dimension  $M \times M$  and with the same rank  $r$  as  $\mathbf{X}$  because for real matrices  $\text{rank}(\mathbf{X} \mathbf{X}^T) = \text{rank}(\mathbf{X}^T \mathbf{X}) = \text{rank}(\mathbf{X})$ . Each matrix element

$$(\mathbf{S}_s)_{mp} = \frac{1}{N} \sum_{n=1}^N \frac{\left( f^{(m)}(n) - \langle f^{(m)} \rangle \right) \left( f^{(p)}(n) - \langle f^{(p)} \rangle \right)}{\sigma^{(m)} \sigma^{(p)}}, \quad (17)$$

is obtained by integrating out the time degree of freedom. The matrix element  $(\mathbf{S}_s)_{mp}$  is called the Pearson or cross-correlation coefficient and gives the overlap between the fluctuations of time series  $f^{(m)}(n)$  and  $f^{(p)}(n)$ . If the time series correspond to the time evolution of observables measured at different locations  $(x_m, y_m)$  and  $(x_p, y_p)$ , then  $(\mathbf{S}_s)_{mp}$  quantifies the spatial correlation that exists in the multivariate time series between these different locations. The diagonal matrix elements are autocorrelation coefficients and  $(\mathbf{S}_s)_{mm} = 1$ . Combining eqs. (15) and (19), we obtain,

$$\begin{aligned} \mathbf{S}_s &\propto (\mathbf{U} \mathbf{\Sigma} \mathbf{V}^T) (\mathbf{U} \mathbf{\Sigma} \mathbf{V}^T)^T \\ &\propto (\mathbf{U} \mathbf{\Sigma} \mathbf{V}^T) (\mathbf{V} \mathbf{\Sigma}^T \mathbf{U}^T) \\ &\propto \mathbf{U} \mathbf{\Sigma} \mathbf{\Sigma}^T \mathbf{U}^T, \end{aligned} \quad (18)$$

such that  $\vec{u}_k = (u_{k1}, u_{k2}, \dots, u_{kM})$  are the eigenvectors of  $\mathbf{S}_s$  with  $k = 1 \dots r$  with associated eigenvalues  $\lambda_k = \sigma_k^2$ . The eigenvectors  $\vec{u}_k$  can be interpreted as the spatial eigen-modes of the multivariate time series  $\mathbf{X}$ , because they give information on the correlations between the  $m = 1 \dots M$  different observables. Because of the matrix property  $\text{trace}(\mathbf{S}_s) = \sum_k \lambda_k$ , where  $\text{trace}(\mathbf{S}_s) = M$  corresponds with the total variance of the multivariate time series  $\mathbf{X}$ , the eigenvalues  $\lambda_k$  can now be given the physical interpretation of *partial variances*: the multivariate time series  $\mathbf{X}$  is decomposed in spatial eigen-modes  $\vec{u}_k$ , each of which is responsible for a part  $\lambda_k$  of the original total variance  $\sum_k \lambda_k$ .

### 2.2.3. Temporal correlation matrix

In an analogue way, the temporal correlation matrix can be defined as

$$\mathbf{S}_t = \frac{1}{M} \mathbf{X} \mathbf{X}^T, \quad (19)$$

with dimension  $N \times N$  and with rank  $r$ . Each matrix element  $(\mathbf{S}_t)_{ni}$  is obtained by integrating out the spatial degree of freedom and calculating the correlation between

the configuration of the system at time moments  $n$  and  $i$ . Combining eqs. (15) and (19), we obtain,

$$\mathbf{S}_t \propto \mathbf{V}\mathbf{\Sigma}^T\mathbf{\Sigma}\mathbf{V}^T, \quad (20)$$

such that  $\vec{v}_k = (v_{k1}, v_{k2}, \dots, v_{kN})$  are the eigenvectors of  $\mathbf{S}_t$  with the same associated eigenvalues or partial variances  $\lambda_k$ , with  $k = 1, \dots, r$ . The vectors  $\vec{v}_k$  can now be interpreted as the temporal eigen-modes of the multivariate time series  $\mathbf{X}$ .

### 2.3. Singular Value Decomposition (SVD) applied to human electroencephalographs (EEG)

In this subsection, we will apply SVD to data from human electroencephalography (EEG). A number of  $M$  electrodes are placed on the head on specific locations to monitor the function of different brain lobes. At any moment  $t = t_0$ , the EEG constitutes a snapshot of a static spatial configuration that exists between the different channels, and in general we will see groups of neighboring channels that exhibit similar activity, see Fig. 2.

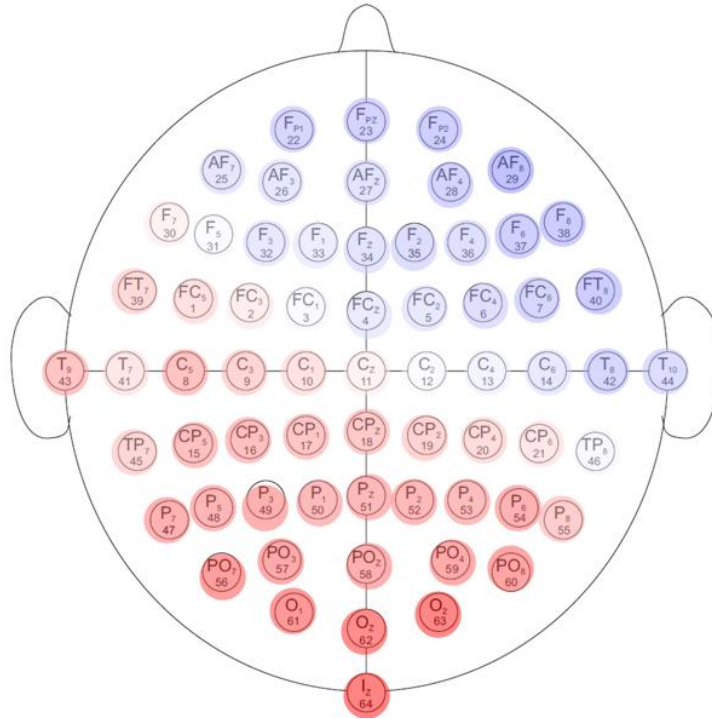


**FIGURE 2.** Electroencephalography (EEG) as an example of a multivariate time series. Location of 64 electrodes in the international 10-20 system. Most electrodes are named after the cerebral lobe that they monitor, F (frontal), T (temporal), P (parietal), O (occipital), whereas C stands for central but there is no central lobe. Odd (even) numbers stand for left (right). The voltage as observed by all electrodes at the specific time  $t = t_0$  is color coded (blue  $V < 0$ , red  $V > 0$ ). Time  $t = t_0$  corresponds with the end of the second eye-blink artifact of Fig.

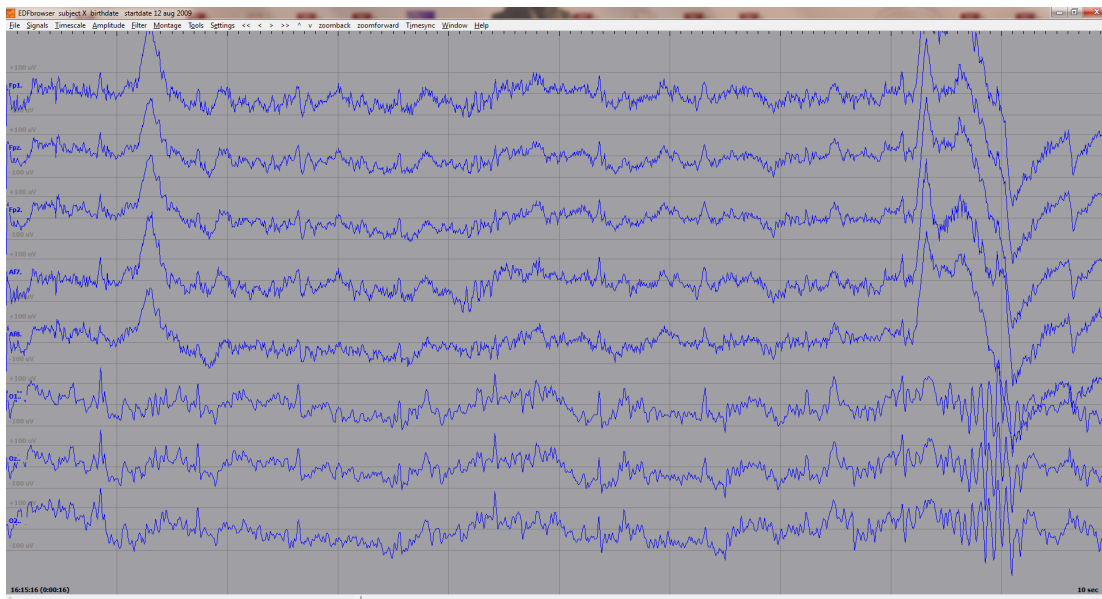


**FIGURE 3.** Electroencephalography (EEG) as an example of a multivariate time series. Fragment of  $\Delta t = 10$ s of time series of voltage fluctuations as seen by (from top to bottom) the Fp1, Fpz, Fp2, Fp7, Fp8, O1, Oz and O2 electrodes. Vertical (horizontal) gridlines are 1s ( $100\mu V$ ) apart. The subject has his eyes open. Most of the voltage fluctuations are spontaneous brain activity. Eye blinking artifacts are observed in the frontal channels at the beginning and end of the fragment. A short episode of dominant alpha rhythm is observed in the occipital channels after the second eye-blinking artifact. Public data from *Physionet* [2, 3].

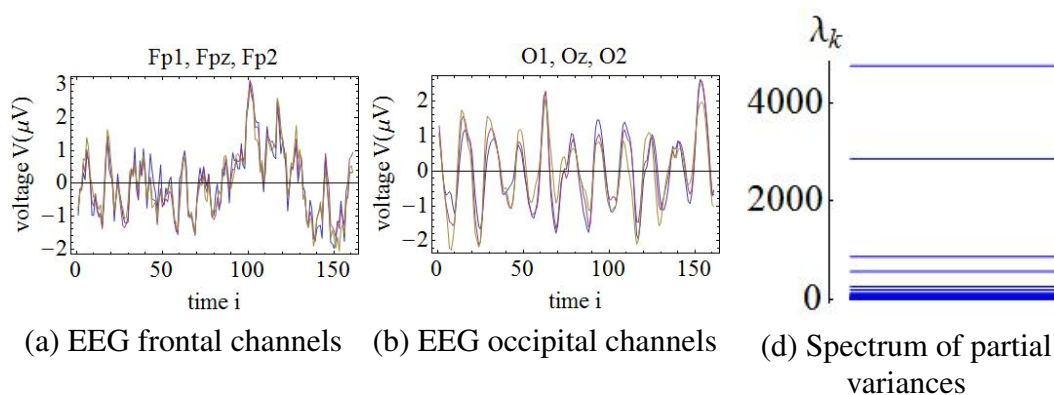
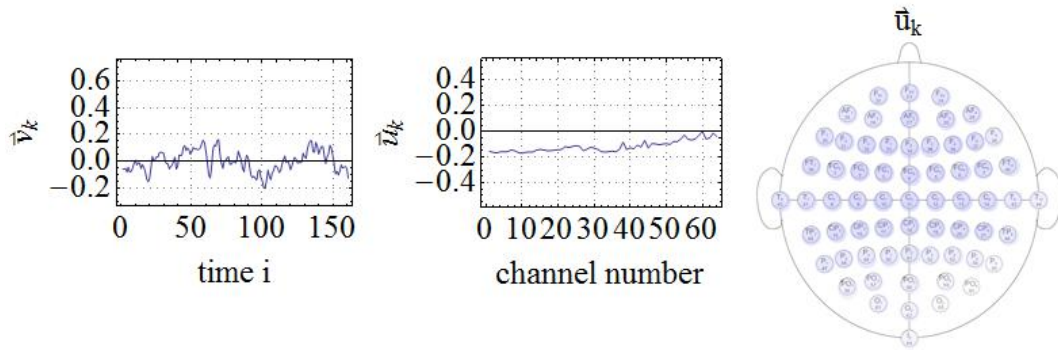
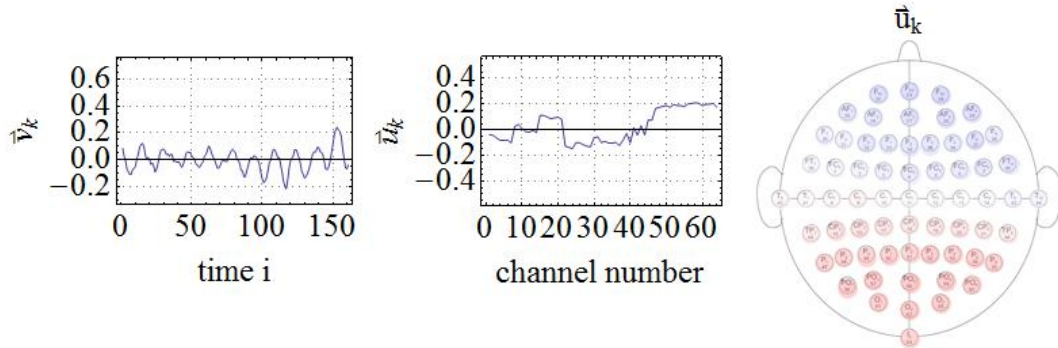


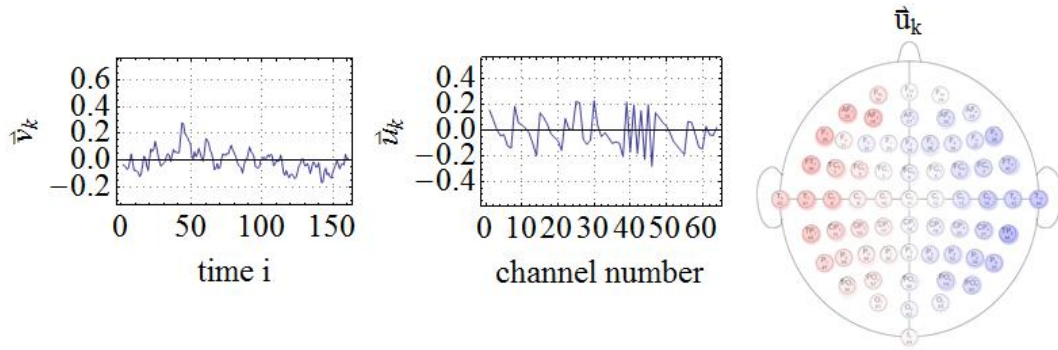
**FIGURE 4.** SVD analysis of a fragment of  $\Delta t = 1$ s of an EEG recording with 64 electrodes and sampling frequency  $f_s = 160$ Hz. The subject has his eyes closed. (a) Time series of frontal channels (Fp1, Fpz, Fp2), the broad peak at  $i = 100$  is an eye movement artifact. (b) Time series of occipital channels (O1, Oz, O3), the periodic behavior with  $f = 10$ Hz is the alpha rhythm. (c) Spectrum of partial variances  $\{\lambda_k, k = 1, \dots, 64\}$ . Public data from *Physionet* [2, 3].



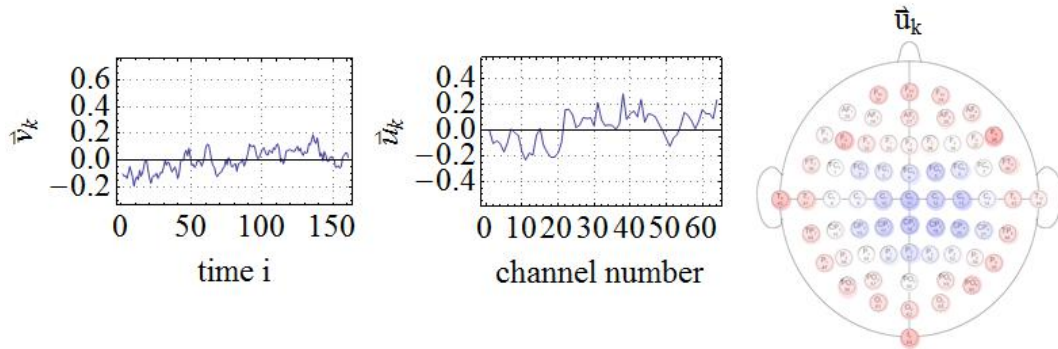
(f) First eigenmode



(g) Second eigenmode



(h) Third eigenmode



(h) Fourth eigenmode

**FIGURE 5.** First few eigen-modes of the SVD analysis of a fragment of  $\Delta t = 1$ s of EEG recording of Fig. 4. The left singular vectors  $\vec{v}_k$  are temporal eigen-modes (left panels), the right singular vectors  $\vec{u}_k$  are spatial eigen-modes (middle and right panels).

On the other hand, an EEG is the result of a dynamical process and the behavior of the time series of the potential fluctuations  $V(t)$  of the different channels can be studied in time, see Fig. 3. In resting conditions, most of the dynamic activity seen in EEG recordings corresponds with spontaneous cerebral activity (stochastic fluctuations), such that only noisy temporal eigen-modes are obtained with an SVD analysis. On the other hand, SVD can be used within the context of Evoked Potentials (EP) to study the standard responses of the brain during stimulation with calibrated visual or acoustic signals [1]. In the following, we will apply SVD to EEG fragments with clearly identifiable eye-blinking artifacts and alpha-wave activity.

Consider the data matrix

$$\mathbf{X} = \begin{pmatrix} f^{(1)}(1) & f^{(1)}(2) & \dots & f^{(1)}(N) \\ f^{(2)}(1) & f^{(2)}(2) & \dots & f^{(2)}(N) \\ \vdots & \vdots & \ddots & \vdots \\ f^{(M)}(1) & f^{(M)}(2) & \dots & f^{(M)}(N) \end{pmatrix}, \quad (21)$$

where the rows correspond with the time series of length  $N = 160$  of  $M = 64$  channels of an EEG recording with a sampling frequency  $f_S = 160\text{Hz}$ , such that  $\mathbf{X}$  corresponds with a fragment of  $\Delta t = 1\text{s}$  of a multivariate time series of electrical cerebral activity. Applying SVD, a spectrum of partial variances is obtained  $\lambda_k$ , and typically the first few partial variances are responsible for almost all of the total variance, see Fig. 4 and ref. [1].

Thus, first of all, SVD constitutes a method for data reduction, because instead of having to deal with the complete data matrix  $\mathbf{X}$  of dimensions  $M \times N$ , the data can be approximated in a good approximation with the first few eigen-modes.

Secondly, the spatial and temporal eigen-modes are often more easy to interpret than the original time series. In Fig. 5, the first few temporal and spatial eigen-modes of the multivariate time series  $\mathbf{X}$  are shown. Each static snapshot of the voltage  $V(t_0)$  at a specific moment  $t = t_0$ , such as panel (a) of Fig. 2, can now be written as a linear superposition of the spatial eigen-modes  $\vec{u}_k$ , and likewise each individual time series  $f^{(m)}(n)$  can be written as a linear superposition of the temporal eigen-modes  $\vec{v}_k$ . Most of the temporal eigen-modes are noisy, but it can be seen that the second temporal eigen-mode  $\vec{v}_2$  corresponds with the alpha rhythm.

### 3. RANDOM MATRIX THEORY (RMT) AND QUANTUM CHAOS

In nuclear physics, at low excitation energies ( $E < 8\text{MeV}$ ), several models exist that explain the nuclear excited states in terms of the properties of the constituent particles of protons and neutrons. At higher excitation energies ( $E > 8\text{MeV}$ ), however, the density of excited states is so large, that it becomes impossible to explain each individual excited state separately. Instead, it is customary to study the statistics of the sequence of levels, whether it corresponds with a random, regular or chaotic series.

To describe the statistics of a quantum excitation spectrum, Wigner invented Random Matrix Theory (RMT) [4]. According to this theory, at high excitation energies, the interactions between the constituent particles of a quantum dynamical system become so

complicated that the exact interaction Hamiltonian can be approximated with a random matrix, where the matrix elements are chosen at random from a predefined probability distribution, with as the only restriction that the matrix should obey the underlying symmetry of the system.

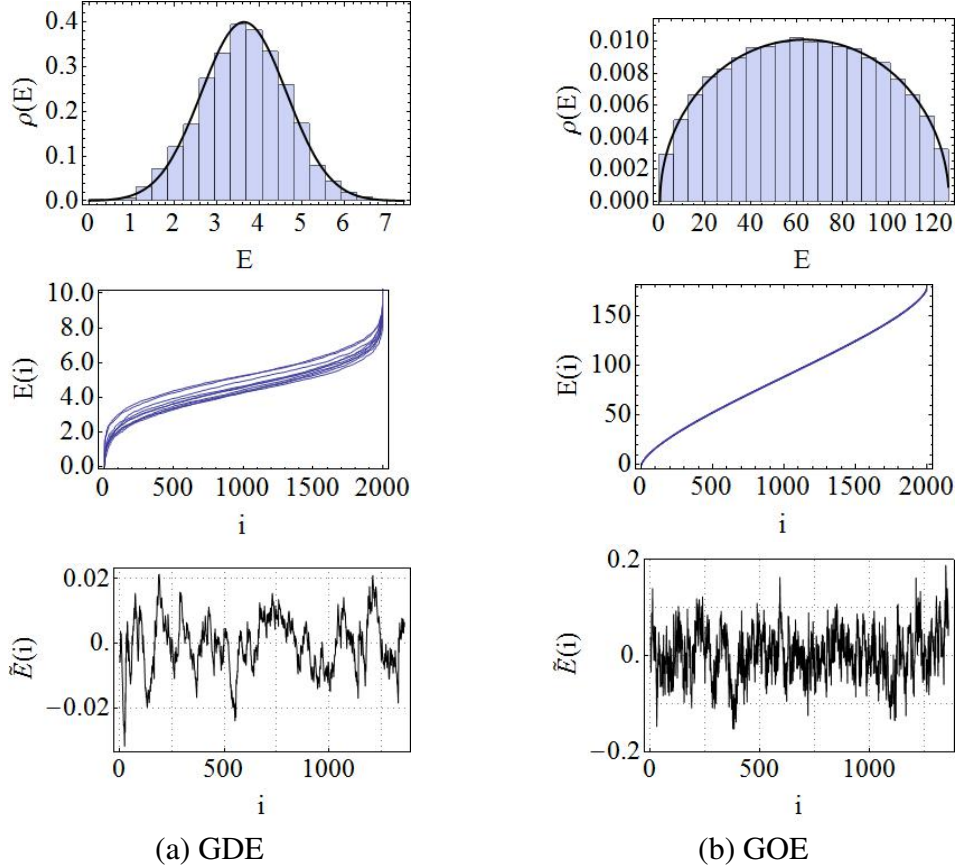


**FIGURE 6.** Two realizations of different random matrix ensembles, the Gaussian Diagonal Ensemble (GDE) (left panels) and Gaussian Orthogonal Ensemble (GOE) (right panels) with  $M = 10$  spectra of  $N = 2000$  levels. (Upper row) The level density  $\rho(E)$  is system dependent, with a gaussian shape for GDE and a semi-circle for GOE. (Middle row) The energy sequence of ordered eigenstates  $E(i) = \bar{E}(i) + \tilde{E}(i)$  with  $i = 1 \dots N$  consists of a global behaviour (trend)  $\bar{E}(i)$  and local fluctuations  $\tilde{E}(i)$ . The trend  $\bar{E}(i)$  is steeper for GOE because of the correlations (level repulsion), which are absent in GDE. The fluctuations  $\tilde{E}(i)$  are not visible on the present energy scale. (Bottom row) Local fluctuations  $\tilde{E}$ , note the difference in scale between the global trend  $\bar{E}(i)$  and the local fluctuations  $\tilde{E}(i)$ .

The majority of the dynamical quantum systems are invariant with respect to time inversion, and their Hamiltonian can be modeled with an ensemble of real symmetrical matrix. The ensemble that results when a gaussian probability distribution is used, is called the Gaussian Orthogonal Ensemble (GOE). After diagonalization of a random matrix, an eigen-spectrum results that offers a statistical description of the excitation spectrum of the quantum system under study. The diagonalization introduces correlations (level repulsion) between the successive eigenstates  $E_1 \leq E_2 \leq \dots E_N$ . GOE describes *quantum chaotic* spectra.

On the other hand, one can construct an ensemble of random diagonal matrices, sometimes called a Diagonal Gaussian Ensemble (GDE) [7]. Diagonal matrices do not need to be diagonalized, and the eigen-spectrum corresponds to only a reordering of the original diagonal elements, so that the sequence of eigenstates that results does not contain correlations. The resulting spectrum is called *integrable*.

An excitation spectrum or eigenspectrum  $E(i) = \bar{E}(i) + \tilde{E}(i)$  with  $i = 1 \dots N$  consists of a dominant global trend  $\bar{E}(i)$  and typically much smaller local fluctuations  $\tilde{E}(i)$ , see Fig. 6. The global trend trivially results because of the energy ordering of the levels, whereas the fluctuations reflect the underlying correlations. Thus, prior to any statistical study, one needs to separate the trend from the fluctuations in a process called *unfolding*.

Another reason for doing the unfolding process is remove the system-dependent features of the spectrum  $E(i)$  and project on an unfolded spectrum  $\varepsilon(i)$  with mean level spacing  $\langle s \rangle = 1$  with  $s(i) = \varepsilon(i) - \varepsilon(i-1)$ . The standard approach to the unfolding process considers the accumulated density function, also called step function, see Fig. 7,

$$\mathcal{N}(E) = \int_{-\infty}^E \rho(E') dE' = \sum_i \theta[E - E(i)], \quad (22)$$

where  $\theta(E)$  is the Heaviside function, and  $\mathcal{N}[E(i)] = i$  gives the number of levels up to  $E = E(i)$ . The step function can be approximated by a smooth function, often a polynomial of arbitrary degree, so that

$$\mathcal{N}(E) = \overline{\mathcal{N}}(E) + \widetilde{\mathcal{N}}(E). \quad (23)$$

The unfolded levels  $\varepsilon(i)$  are given by projection of the actual energies over the smooth function, i.e.

$$\varepsilon(i) = \overline{\mathcal{N}}[E(i)]. \quad (24)$$

By construction, the mean unfolded level spacing becomes,

$$\begin{aligned} \langle s \rangle &= \frac{1}{N-1} \sum_{i=2}^N (\varepsilon(i) - \varepsilon(i-1)) \\ &= \frac{1}{N-1} ((\varepsilon_N - \varepsilon_{N-1}) + (\varepsilon_{N-1} - \varepsilon_{N-2}) + (\varepsilon_{N-2} - \varepsilon_{N-3}) \dots + (\varepsilon_3 - \varepsilon_2) + (\varepsilon_2 - \varepsilon_1)) \\ &= \frac{\varepsilon_N - \varepsilon_1}{N-1} \\ &\approx \frac{N-1}{N-1} = 1. \end{aligned} \quad (25)$$

Here, we have used that for spectra with many levels  $N$  we have,  $\varepsilon_i \approx i$ . Level fluctuations around the system-dependent level density  $\rho(E)$  are transformed in fluctuations around the uniform distribution  $\rho(\varepsilon)$ , see Fig. 7.

The local unfolded level fluctuations can be studied with specialized fluctuation measures. The simplest fluctuation measure is the Nearest-Neighbour Spacing (NNS) distribution. It is simply the normalized histogram  $P(s)$  of all the level spacings  $s(i)$  and quantifies correlations between neighboring levels, it thus corresponds to a short range

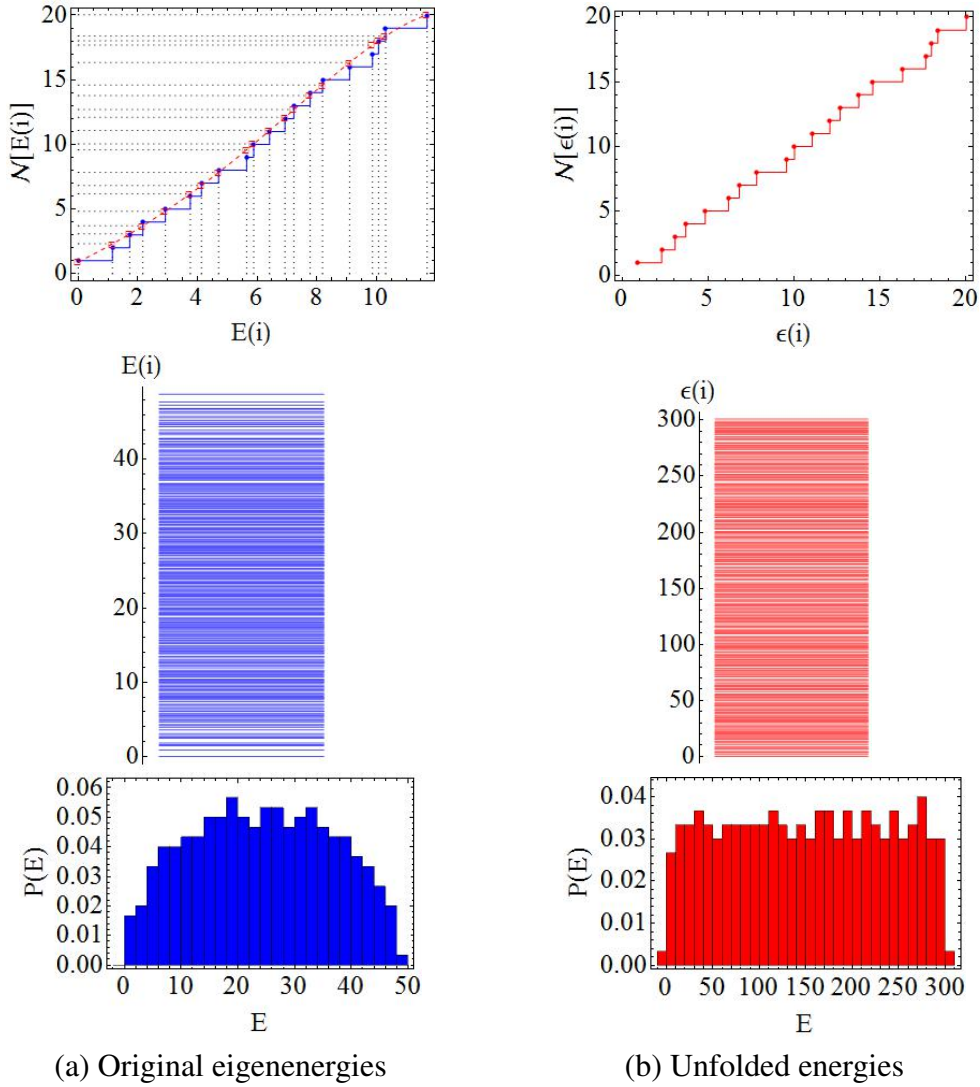


**FIGURE 7.** Traditional approach to the unfolding process, original spectrum  $E(i)$  (left panels) and unfolded spectrum  $\epsilon(i)$  (right panels). (Upper row) The step function of original energies  $\mathcal{N}(E) = \overline{\mathcal{N}}(E) + \widetilde{\mathcal{N}}(E)$  is curved because of the non-constant level density  $\rho(E)$ , whereas the step function of unfolded energies  $\mathcal{N}(\epsilon)$  corresponds with fluctuations around a straight slope. (Middle row) A matrix eigen-spectrum  $E(i)$  is typically more dense for intermediate energies, and less dense at the extremes  $E \ll$  and  $E \gg$ , whereas an unfolded spectrum has a uniform density  $\rho(\epsilon) = 1$ . (Bottom row) The shape of the original level density  $\rho(E)$  is density dependent, whereas the density of the unfolded levels is uniform  $\rho(\epsilon) = 1$ . We are interested in local fluctuations around the uniform density.

statistic. Analytical predictions are known for the GDE and GOE models. In the case of GDE, no correlations (level repulsion) are present in the spectrum, such that both zero spacings and larger spacings can be observed between successive levels, and the distribution can be described by a poissonian exponential behavior. In the case of GOE, correlations (level repulsion) are present, such that zero spacings are highly improbable. Because of the unfolding, for both ensembles the mean level spacings is unitary,  $\langle s \rangle = 1$ .

Analytically, we have,

$$P^{\text{GDE}}(s) = \exp(-s) \quad (26)$$

$$P^{\text{GOE}}(s) = \frac{\pi}{2}s \exp\left(-\frac{\pi}{4}s^2\right). \quad (27)$$

On the other hand, long-range correlations can be measured with the  $\Delta_3(\ell)$  statistic, that quantifies as a function of window size  $\ell$  the variance of the unfolded step function  $\mathcal{N}(\varepsilon)$  around the best fitted straight line, i.e.

$$\Delta_3(\ell) = \text{Min}_{A,B} \left( \frac{1}{\ell} \int_{\varepsilon}^{\varepsilon+\ell} (\mathcal{N}(\varepsilon) - A\varepsilon - B)^2 d\varepsilon \right). \quad (28)$$

For a non-correlated spectrum, also called *soft spectrum*, the variance rises linearly with window size  $\ell$ . Correlations cause *rigidity*, i.e. a suppression of variance for large window sizes. The analytical predictions for GDE and GOE are,

$$\Delta_3^{\text{GDE}}(\ell) = \frac{\ell}{15} \quad (29)$$

$$\Delta_3^{\text{GOE}}(\ell) = \frac{1}{\pi^2} \left( \log(2\pi\ell) + \gamma - \frac{5}{4} - \frac{\pi^2}{8} \right). \quad (30)$$

The results for the spectral fluctuation measures for a specific system of interest with unknown underlying symmetry can be compared with the analytical predictions of models with known symmetries. In Fig. 8, short-range  $P(s)$  and long-range  $\Delta_3(\ell)$  are studied for the  $J^\pi = 4^+$  sub-spectrum of  $^{48}\text{Ca}$ , calculated with the nuclear shell model. Short- and long-range fluctuation measures agree that this nuclear excitation spectrum corresponds with the GOE predictions, and that the underlying symmetry is time-inversion invariance.

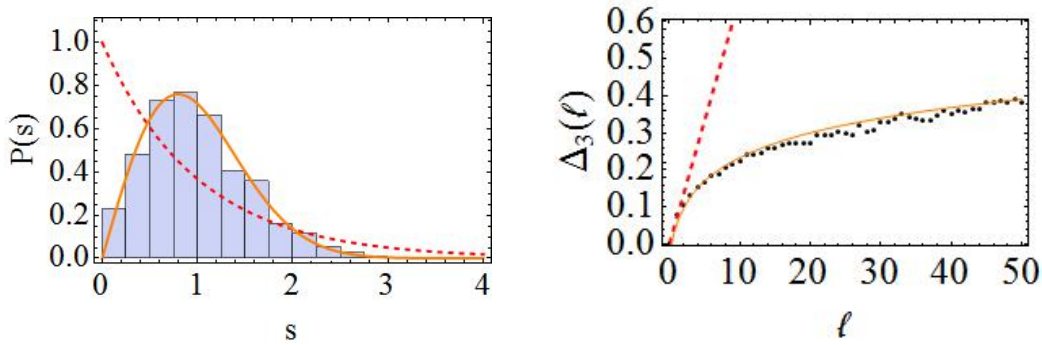


**FIGURE 8.** Comparison of spectral fluctuation measures of the  $J^\pi = 4^+$  sub-spectrum of  $^{48}\text{Ca}$  (bars and dots) with theoretical predictions for GDE (dashed red line) and GOE (continuous orange line). (Left panel) Short-range Nearest-Neighbour Spacing (NNS) distribution  $P(s)$  with  $\langle s \rangle = 1$ . (Right panel) Long-range spectral rigidity measure  $\Delta_3(\ell)$ .

## 4. TIME-SERIES ANALYSIS APPLIED TO RMT

### 4.1. Time-series interpretation of spectral fluctuations and $1/f$ noise

In a recent approach, the unfolded fluctuations of the accumulated level density function  $\widetilde{\mathcal{N}}(E) = \mathcal{N}(E) - \overline{\mathcal{N}}(E)$  (also called  $\delta_n$  function) were interpreted as a time series [6, 7, 8]. This treatment opened the field to the application of specialized techniques from signal analysis, such as Fourier spectral analysis [6, 7, 8, 29], Detrended Fluctuation Analysis (DFA) [9, 10], wavelets [11], Empirical Mode Decomposition (EMD) [12, 13, 14], and normal-mode analysis [15, 16]. The result of these investigations is that for Gaussian RMT ensembles, the fluctuation time series is scale invariant (fractal), which in the Fourier power spectrum is reflected in a power law,

$$P(f) \propto 1/f^\beta, \quad (31)$$

where  $f$  is the frequency of the periodic modes in which the time series is decomposed, whereas when more general non-periodic normal modes are used, such as the temporal modes of Fig. 5, a “generalized power spectrum” or so-called “scree diagram” results,

$$\lambda_k \propto 1/k^\gamma, \quad (32)$$

where  $k$  is the index of the normal modes, and where  $\beta = \gamma = 2$  (Poisson limit) and  $\beta = \gamma = 1$  (GOE limit), such that the power law does not seem to depend on the basis used to decompose the time series [17].

### 4.2. Data-adaptive unfolding

#### 4.2.1. Data-adaptive unfolding of ensembles of spectra

All the fluctuation measures mentioned so far, including the traditional measures such as NNS and  $\Delta_3$ , and the time-series based measures of Fourier power spectrum  $P(f)$ , DFA, EMD and normal modes, are calculated after the prior technical step of unfolding of the original eigenvalues. Some of the possible unfolding techniques are polynomial unfolding, local averaging, Gram-Charlier expansion and the constant-temperature formula [5]. However, the statistical results for the fluctuations can be quite sensitive on the specific unfolding procedure used, as mentioned in the context of quantum chaos [18], but also in more recent applications in network analysis [19].

A similar problem in the context of signal analysis is how to define the trend of a non-stationary time series. It was concluded that the trend is an intrinsic property of the time series that should not be defined arbitrarily by an external observer, but should be obtained in a data-adaptive way from the data itself, see ref. [20]. The purpose of the present section is twofold: first, we propose to interpret the spectrum of original eigenvalues  $E(n)$  directly as a time series, such that data-adaptive techniques from signal analysis can be used to decompose the sequence in a global and local part,

$$E(n) = \overline{E}(n) + \widetilde{E}(n), \quad (33)$$

secondly, we will present one particular method based on SVD with which this unfolding can be realized. We will see that the power law of eq. (32) is obtained already during the proposed data-adaptive unfolding procedure.

A spectrum is a monotonous function that has a dominant trend, with superposed fluctuations that are typically orders of magnitude smaller. Consequently, the variability of a spectrum will be due principally to its trend components, characterized by very large partial variances  $\lambda_k$ , whereas the fluctuation components will be associated with much smaller partial variances. We thus expect to be able to distinguish in a data-adaptive way in the scree diagram between the trend and the fluctuations. To fix the ideas, consider a GDE and a GOE ensemble of  $m = 1 \dots M$  eigen-spectra  $E^{(m)}(n)$ , where each spectrum consists of  $n = 1 \dots N$  levels. Each spectrum is conveniently accommodated in a row of the  $M \times N$  dimensional matrix  $\mathbf{X}$ , which can now be interpreted as a multivariate time series such as in eq. (21). After applying SVD to  $\mathbf{X}$ , a scree diagram is obtained where the first few partial variances are orders of magnitude larger than the higher order partial variances and thus correspond to the trend series  $\bar{E}(n)$ , see Fig. 9. The higher-order partial variances, associated to the fluctuation series  $\tilde{E}(n)$ , follow the power law of eq. (32) with  $\gamma = 2$  in the GDE case and  $\gamma = 1$  in the GOE case. If the Fourier power spectrum is calculated from the fluctuation time series  $\tilde{E}(n)$ , then the power law of eq. (31) follows with  $\beta = 2$  in the GDE case and  $\beta = 1$  in the GOE case.

## 5. RANDOM MATRIX THEORY (RMT) APPLIED TO MULTIVARIATE STATISTICS

### 5.1. RMT spectral fluctuation measures applied to multivariate statistics in finance, networks, the climate and electro- (EEG) and magnetoencephalography (MEG)

In a previous section, SVD was applied to data from an EEG recording. Typically, in multivariate statistics, the first few partial variances  $\lambda_k$  are orders of magnitude larger than the higher-order ones, see Fig. 4. Thus, it is assumed that a multivariate time series can be approximated by the first few dominant eigen-modes, whereas the higher-order components are neglected as noise. However, when the correlation matrices are calculated from fragments of EEG data, such as in Fig. 10, then the resulting scree diagram of ordered partial variances  $\lambda_k$  typically behaves as a power law  $\lambda_k \propto 1/k^\gamma$ , as can be seen in Fig. 11, suggesting that higher-order modes do significantly contribute to the dynamics. Recently, in the context of correlation matrices of financial multivariate statistics, it was suggested that the whole spectrum of partial variances  $\lambda_k$  with  $k = 1, \dots, r$  may contain useful information, and that the spectral fluctuation measures from RMT can be applied to obtain this information [24, 25, 26]. The approach arouse a lot of interest in many different fields, such as in the study of eigen-spectra of adjacency matrices of networks [27, 28, 29], and eigen-spectra of empirical correlation matrices in the climate [30], and electro- and magnetoencephalography [31, 32, 33, 34].

In the application to human EEG of ref. [32], spectral fluctuations of correlation matrices were compared between subjects in rest (eyes open) were vs. visually stimulated

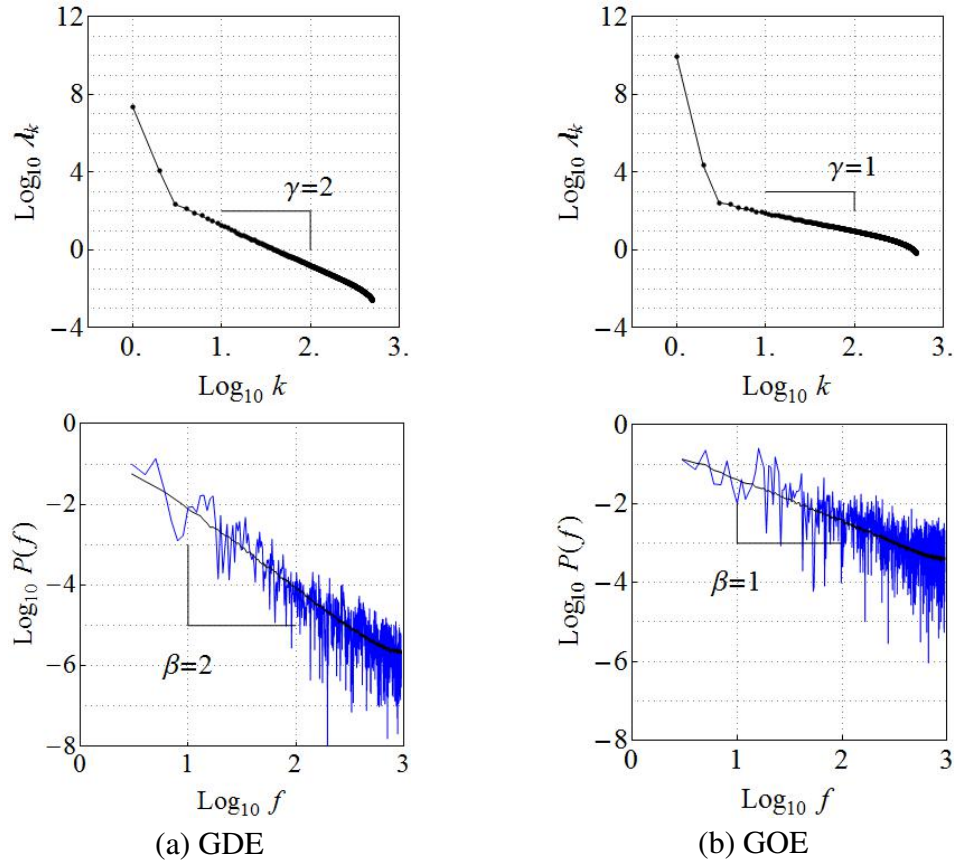


**FIGURE 9.** Results of the application of SVD to a GDE and GOE ensemble of  $M = 500$  spectra, each with  $N = 2000$  levels. (Upper row) Scree diagram of ordered partial variances  $\lambda_k$ , of which  $\lambda_1$  and  $\lambda_2$  correspond to the trend  $\bar{E}^{(m)}(n)$ , whereas  $\lambda_k$  with  $k = 3 \dots r$  correspond to the fluctuations  $\tilde{E}^{(m)}(n)$  and follow a power law  $\lambda_k \propto 1/k^\gamma$  with  $\gamma = 2$  (Poisson) and  $\gamma = 1$  (GOE). (Bottom row) The Fourier power spectrum of the fluctuations  $\tilde{E}^{(m)}(n)$  follows a power law  $P(f) \propto 1/f^\beta$  with  $\beta = \gamma = 2$  (Poisson) and  $\beta = \gamma = 1$  (GOE), shown for one particular spectrum realization (blue curve) and for the ensemble mean (black curve). Adapted from [21].

subjects. No difference was observed for the NNS statistic, which was to follow the GOE prediction. In the case of the number variance  $\Sigma_2$  statistic, GOE was found for subjects in rest, whereas a deviation towards GDE was found for the visually stimulated subjects. The interpretation was that the visual stimulation changes the correlation pattern of the data due to its large response in the visual cortex. As a consequence, its relative correlations with the remaining parts of the cortex are lowered. These changes are too subtle to influence the short-range NNS distribution, whereas the long-range  $\Sigma_2$  statistic was sensitive enough to detect the change.

The application in networks of ref. [28] makes the physical meaning more obvious. A network was considered, consisting of two subnetworks, and was represented with its *adjacency matrix*. For an unweighted network, the adjacency matrix  $\mathbf{A}$  is determined in the following way. If the nodes  $i$  and  $j$  are connected, then  $A_{ij} = 1$  and 0 otherwise. For an undirected network, this matrix is symmetric and consequently has real eigenvalues.

The spectral fluctuations of the adjacency matrix, as appreciated with the short-range NNS statistic, corresponded with the GDE prediction when no connections were present between the two subnetworks, but converged rapidly towards GOE for small connection probabilities. On the other hand, the long-range  $\Delta_3$  statistic remained close to the GDE limit for small connection probabilities and needed large probabilities in order to converge towards the GOE limit.

## 5.2. Network interpretation of RMT fluctuation measures

Here, we consider two short fragments of  $\Delta t = 1$ s of EEG recordings with  $M = 64$  electrodes, time-series length  $N = 160$  and sampling frequency  $f_s = 160$ Hz. The first data set corresponds with a person with eyes open and without artifacts, and all recorded time series correspond with noisy spontaneous cerebral activity. The second data set corresponds with a person with eyes closed, eye-movement artifacts as appreciated in the frontal channels and alpha rhythm in the occipital channels.

The resulting spatial correlation matrices  $\mathbf{S}_s$  are shown in Fig. 10. In the eye-open case, correlations extend over the whole correlation matrix, whereas in the eyes-closed case frontal channels anticorrelate slightly with the occipital channels.

The difference in configuration is even better observed in the associated binary adjacency matrix, obtained by truncating the correlation matrix (taking arbitrarily 0 if  $|(\mathbf{S})_{ij}| < 0.5$  and 1 if  $|(\mathbf{S})_{ij}| \geq 0.5$ ). Here, it can be seen that in the eyes-closed case the occipital channels disconnect from the frontal channels. The graph representation visualizes the differences observed in the adjacency matrix for the two cases. In the eyes-open case, the brain corresponds with an almost completely connected network, whereas in the eyes-closed case, the network consists of two subnetworks (frontal vs. occipital) that are partially disconnected. The approach is based on the evidence that there are functional, i.e. non-physical, connections in the brain, that can be discovered the synchronicity between cerebral time series from different areas [35, 36, 37]. In this way, changes in dynamical brain networks have been discovered in alzheimer and stroke patients [38, 39].

The changes in network structure can also be studied using the spectral fluctuation measures of RMT, see Fig. 11. The spectrum of partial variances  $\lambda_k$  first needs to be unfolded using the step function  $\mathcal{N}(\lambda_k)$ , whereas now the step function goes down because of the large-to-small ordering of the partial variances. In the present case, the unfolding is done using a polynomial of order 3. The step function of unfolded energies  $\mathcal{N}(\epsilon_k)$  shows the expected fluctuations around a straight line. The short-range NNS statistic does not detect any difference between the eyes-open and the eyes-closed case, and in both cases follows the GOE prediction. The long-range  $\Delta_3$  statistic corresponds with the GOE prediction in the eyes-open case, indicating a fully connected network. In the eyes-closed case, the  $\Delta_3$  statistic shows a deviation towards the GDE prediction, indicating the presence of (partially) disconnected subnetworks, in correspondence with the results obtained using adjacency matrices and network analysis.

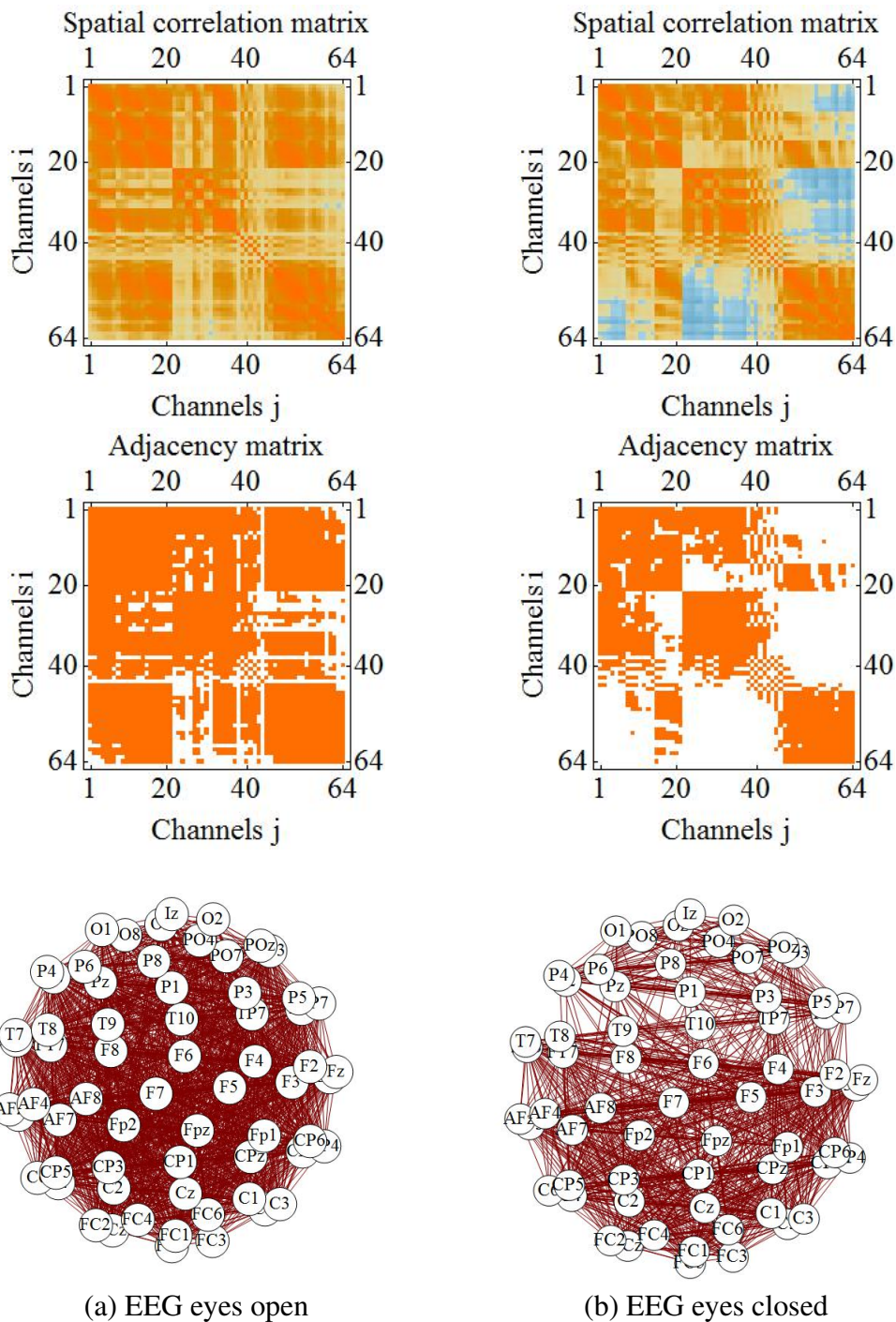


**FIGURE 10.** Network interpretation of a fragment of  $\Delta t = 1$  s of EEG data, of a person with eyes open and without eye-blinking artifacts (left panels), and of the person with eyes closed, eye movement artefact and alpha rhythm from Fig. 4 and 5 (right panels). (Upper row) Spatial correlation matrix  $S_i = \frac{1}{N} \mathbf{X}_i \mathbf{X}_i^T$ . (Second row) Binary adjacency matrix obtained by truncating the correlation matrix. (Bottom row) Graph representation of the adjacency matrix. In the eyes-open case, all channels observe spontaneous cerebral activity and correlations are similar between all time series. The resulting dynamical network is well connected. In the eyes-closed case, frontal channels observe the eye-movement artifact and occipital channels observe alpha rhythm, such that correlations are stronger within the former and latter groups, and weaker between both groups. The resulting dynamical network consists of two subnetworks. Public data from *Physionet* [2, 3].

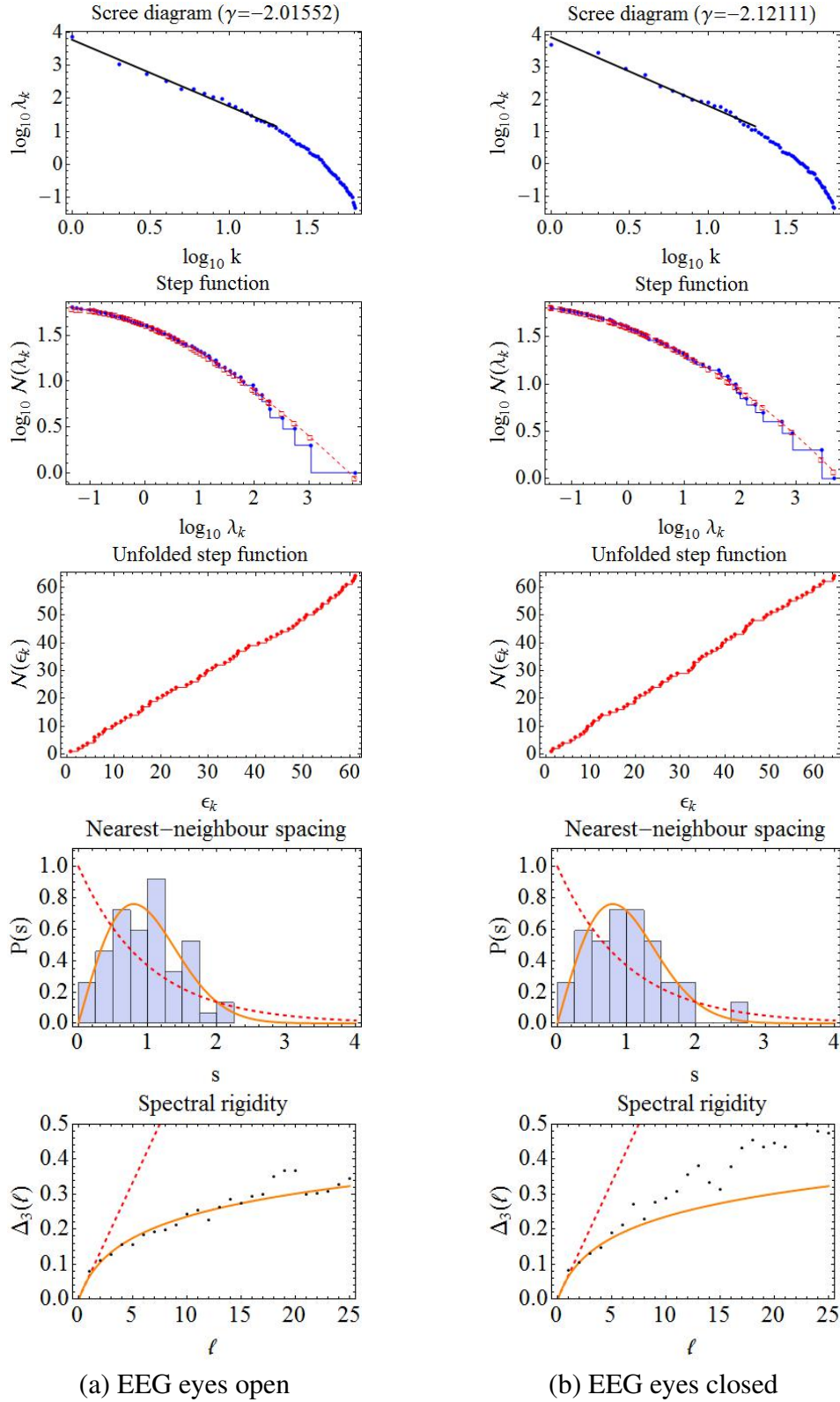


**FIGURE 11.** RMT analysis of the spectral fluctuations of the partial variances of the EEG correlation matrices of Fig. 10. (Upper row) Scree diagram of partial variances  $\lambda_k$ . (Second row) Step function  $\mathcal{N}(\lambda_k) = k$  with polynomial smooth fit. (Third row) Unfolded step function  $\mathcal{N}(\varepsilon_k) = k$ . (Fourth row) Nearest-neighbor spacing (NNS) distribution. (Bottom row)  $\Delta_3$  spectral rigidity function. In the panels with NNS and  $\Delta_3$ , experimental results (histogram bars and dots) are compared with theoretical predictions of GDE (red dashed line) and GOE (orange continuous line).

## 6. CONCLUSIONS

It is interesting to note that the primary focus of the application of RMT in the field of quantum chaos was to find relations between chaotic behavior in the classical and the quantum world. On the other hand, the recent applications of RMT to multivariate statistics, e.g. in finance or human EEG, and the application of time-series analysis in RMT, have as a focus complexity and the statistical behavior of composite dynamical systems. Perhaps these new applications will shed a new light on the understanding of quantum chaos.

## ACKNOWLEDGMENTS

Financial support is acknowledged from CONACYT (grants CB-2011-01-167441, CB-2010-01-155663 and I010/266/2011/C-410-11), PAPIIT-DGAPA (grant IN114411), the European Commission (project FP7-PEOPLE-2009-IRSES-247541-MATSIQEL) and the Instituto Nacional de Geriatria (project DI-PI-002/2012). The author wishes to thank G. Torres Vargas, J. C. López Vieyra, L. Aide Álvarez and O. Bureos Lecona for fruitful discussions.

## REFERENCES

1. R.N. Harner and S. Riggio, *Brain Topogr.* **2** (1989) 91-98.
2. A. L. Goldberger, L.A.N. Amaral, L. Glass, et al, *Circulation* **101** (2000) e215-20 [<http://www.physionet.org/physiobank/database/eegmidb/>]
3. G. Schalk, D.J. McFarland, T. Hinterberger, et al, *IEEE Trans. on Biomed. Engin.* **51** (2004) 1034.
4. M.L. Mehta, *Random Matrices* (2nd Ed.), Academic Press, New York, 1991.
5. M.S. Bae, T. Otsuka, T. Mizusaki and N. Fukunishi, *Phys. Rev. Lett.* **69** (1992) 2349.
6. J. Gómez, K. Kar, V.K.B. Kota, et al, *Phys. Rep.* **499** (2011) 103.
7. A. Relaño, J.M.G. Gómez, R.A. Molina, J. Retamosa and E. Faleiro, *Phys. Rev. Lett.* **89** (2002) 244102.
8. E. Faleiro, J.M.G. Gómez, R.A. Molina, L. Muñoz, A. Relaño and J. Retamosa, *Phys. Rev. Lett.* **93** (2004) 244101.
9. M.S. Santhanam, J.N. Bandyopadhyay and D. Angom, *Phys. Rev. E* **73** (2006) 015201(R).
10. E. Landa, I. Morales, C. Hernández, J. C. López Vieyra and A. Frank, *Rev. Mex. Fís. S* **54** (2008) 48.
11. C. Male, G. Le Caër and R. Delannay, *Phys. Rev. E* **76** (2007) 042101.
12. E. Landa, I. Morales, R. Fossion, P. Stránský, V. Velázquez, J. C. López Vieyra and A. Frank, *Phys. Rev. E* **84** (2011) 016224.
13. I. O. Morales, E. Landa, P. Stránský and A. Frank, *Phys. Rev. E* **84** (2011) 016203.
14. E. Landa, I. Morales, P. Stránský and A. Frank, *Phys. Rev. E* **87** (2013) 032919.
15. A. Andersen, A. D. Jackson and H.J. Pedersen, *Nucl. Phys. A* **650** (1999) 213.
16. A.D. Jackson, C. Mejia-Monasterio, T. Rupp, M. Saltzer and T. Wilke, *Nucl. Phys. A* **687** (2001) 405.
17. J.B. Gao, Y. Cao and J.-M. Lee, *Phys. Lett. A* **314** (2001) 392.
18. J.M.G. Gómez, R. A. Molina, A. Relaño and J. Retamosa, *Phys. Rev. E* **66** (2002) 036209.
19. S.M. Abuelin and A.Y. Abul-Magd, *Pocedia CS* **12** (2012) 69.
20. Z. Wu, N.E. Huang, S.R. Long et al., *Proc. Nat. Acad. Sci.* **104** (2007) 14889.
21. R. Fossion, G. Torres Vargas and J.C López Vieyra, to appear in *Phys. Rev. E*.
22. G. Torres Vargas, R. Fossion, V. Velázquez and J.C. López Vieyra, to appear in *J. Phys.: Conf. Ser.*
23. R. Fossion, G. Torres Vargas and J.C. López Vieyra, submitted to *Phys. Rev. E*.
24. L. Laloux, P. Cizeau, J.-P. Bouchaud and M. Potters, *Phys. Rev. Lett.* **83** (1999) 1467.
25. V. Plerou, P. Gopikrishnan, B. Rosenow, et al., *Phys. Rev. Lett.* **83** (1999) 1471.
26. V. Plerou, P. Gopikrishnan, B. Rosenow, et al., *Phys. Rev. E* **65** (2002) 066126.

27. F. Luo, J. Zhong, Y. Yang and J. Zhou, *Phys. Rev. E* **73** (2006) 031924.
28. S. Jalan, *Phys. Rev. E* **80** (2009) 046101.
29. Y. Bin, L. Hui-jun and M. Xiao-ping, *Phys. A* **389** (2010) 5328.
30. M.S. Santhanam and P.K. Patra, *Phys. Rev. E* **64** (2001) 016102.
31. J. Kwapień, S. Drożdż and A.A. Ioannides, *Phys. Rev. E* **62** (2000) 5557.
32. P. Šeba, *Phys. Rev. Lett.* **91** (2003) 198104.
33. M. Müller, Y. López Jiménez, C. Rummel, G. Baier, A. Galka, U. Stephani and H. Muhle, *Phys. Rev. E* **74** (2006) 041119.
34. A. Koutras, G.K. Kostopoulos and A.A. Ioannidis, *IEEE Trans. Biomed. Engin.* **55** (2008) 957.
35. O. Sporns, D.R. Chialvo, M. Kaiser and C.C. Hilgetag, *Trends Cogn. Sci.* **8** (2004) 418.
36. E. Bullmore and O. Sporns, *Nature Rev. Neurosci.* **10** (2009) 186.
37. O. Sporns, *Networks of the brain*, MIT Press, Cambridge, 2011.
38. C.J. Stam, B.F. Jones, G. Nolte, et al., *Cereb. Cortex* **17** (2007) 92.
39. F. De Vico Fallani, L. Astolfi, F. Cincotti, et al., *Anatom. Rec.* **292** (2009) 2023.